(Received 13 January 2025, Accepted 20 February 2025, Scheduled 13 March 2025)

Advanced Helical Antenna Design for X-Band Applications Using AI

Mohammed Yousif Zeain[1], Maisarah Abu[1], Apriana Toding[2], Zahriladha Zakaria[1], Hussein Alsariera[1], Ihsan Ullah[3], Ali Abdulateef Abdulbari[4], Hamizan Yon[5], Bilal Salman Taha[6, 7], and Muhammad Inam Abbasi[1, *]

[1]*Centre for Telecommunication Research and Innovation (CeTRI) Faculty of Engineering and Technology Electronics and Computer (FTKEK) Universiti Teknikal Malaysia Melaka (UTeM), Hang Tuah Jaya, 76100 Durian Tunggal, Melaka, Malaysia*
[2]*Department of Electrical Engineering, Univeristas Kristen Indonesia Paulus (UKIP), Makassar, Indonesia*
[3]*Department of Computer Science and Engineering, Yuan Ze University, Taoyuan, Taiwan*
[4]*Information Technology Center, University of Technology, Baghdad, Iraq*
[5]*Antenna Research Center College of Engineering, School of Electrical Engineering, Universiti Teknologi MARA, Malaysia*
[6]*Department of Electrical and Electronics, University Tenaga National, Malaysia*
[7]*Institute of Microengineering and Nanoelectronics (IMEN), Universiti Kebangsaan Malaysia (UKM), Malaysia*

ABSTRACT: This paper presents the design, fabrication, and characterization of a novel 3D-printed helical antenna operating within the 9.4–10.8 GHz frequency band. The antenna, employing a lightweight paper substrate and a strip-based helical structure, exhibits robust circular polarization characteristics and wideband operation. Rigorous simulations predict a peak CP gain of 11.7 dBi at 9.8 GHz and a high simulated radiation efficiency of 95%. Experimental measurements validate these predictions, achieving a peak CP gain of 11.6 dBi at 9.8 GHz. This research demonstrates the potential of 3D-printed helical antennas for diverse applications in modern wireless communication systems, including 5G, satellite communication, and radar. Furthermore, this study leverages the power of Artificial Intelligence (AI) by employing the Grey Wolf Optimizer (GWO), a sophisticated metaheuristic algorithm, to optimize the antenna's design. The GWO algorithm is utilized to efficiently search the design space and identify optimal values for key parameters, such as the number of turns, helix pitch, and helix diameter, with the objective of maximizing antenna gain to achieve a target of 15 dBi. This research highlights the potential of AI-driven optimization techniques in advancing the design of high-performance antennas for emerging wireless communication systems.

1. INTRODUCTION

Wireless communication systems, including those used in satellite, navigation, mobile, and radar applications [1], have undergone rapid development. These modern systems often necessitate antennas with specific characteristics: broadband operation, circular polarization (CP), affordability, lightweight design, and seamless integration with radio frequency front-end components [2, 3].

CP antennas exhibit several advantages over linearly polarized (LP) antennas, including reduced polarization mismatch and the ability to mitigate ionospheric depolarization in satellite systems [4]. Helical antennas find diverse applications in global positioning satellites, satellite ground stations [5], and medical and healthcare sectors. A conventional helical antenna comprises a single conductor wound into a helical shape and can operate in three distinct modes: normal, axial, and conical. Axial-mode helical antennas are particularly advantageous for their ability to radiate end-fire CP electromagnetic waves across a broad frequency spectrum. Conductor loss in conventional wire-made helical antennas significantly degrades radiation efficiency, particularly at higher frequencies. Radiation efficiency is a critical factor for optimizing reliability, operating bandwidth, and gain in wireless communication systems [1–5]. The integration of antennas with radio frequency circuits is an essential aspect of contemporary communication systems. Research has explored the use of dielectric-based helical antennas [6, 7] fabricated using printed copper strips on flexible substrates that are subsequently rounded to form a helical shape [8]. High-permittivity materials can be utilized to reduce the physical size of these antennas. However, integrating high-permittivity materials with other components of radio frequency (RF) front ends can present significant challenges [9].

The helical antenna described in [10], operating in the 5.8–5.9 GHz band, was constructed using a 1.5 mm thick Teflon substrate and a strip-line configuration. This design achieved a maximum directivity of 12.2 dB at 5.8 GHz and 13.1 dB at 5.9 GHz, with corresponding peak gains of 11.25 dB and 12.6 dB, respectively. While these results are commendable, further optimization efforts could potentially lead to even greater performance. This work presents a planar substrate-based axial-mode helix antenna with wide impedance and axial ratio bandwidths. This design simplifies fabrication

* Corresponding author: Muhammad Inam Abbasi (inamabbasi@utem.edu.my).

and solves impedance-matching issues. The antenna exhibits a 1.37 GHz impedance bandwidth (1.56–2.93 GHz) and a 1.18 GHz axial ratio bandwidth (1.58–2.76 GHz), suitable for L- and S-band satellite communication. It achieves a peak gain of 11.3 dBi at 1.6 GHz [11]. This article presents a compact axial-mode helical antenna (AMHA) utilizing spoof surface plasmon polaritons (SSPPs). By leveraging the slow-wave properties of SSPPs, the antenna achieves significant size reduction compared to traditional designs. This SSPP-based AMHA demonstrates high gain, low cost, and simple processing, making it suitable for improving system integration in wireless communication [12]. This article presents a wideband circularly polarized reflector array antenna (RAA) utilizing dual-branch helical antennas as reflecting elements for high-power microwave (HPM) radiation. The proposed RAA significantly enhances bandwidth, beam-scanning, and beam-forming capabilities compared to conventional HPM antennas. Furthermore, it offers the potential for flexible and conformal array configurations [13]. This paper introduces a novel, compact, wideband phased array active helical antenna designed for monitoring high-frequency interference. The proposed antenna array overcomes the size limitations of traditional multi-element high frequency (HF) antenna designs. Notably, the front-to-back ratio of this circularly polarized phased array surpasses 20 dB across its operational range. This array facilitates the simultaneous monitoring of both vertically and horizontally polarized signals, providing a practical alternative to larger antennas, particularly in scenarios with limited space [25]. Multifilar helical antennas, comprising multiple helical elements fed with appropriate phase differences, can generate circular polarization. These antennas have found widespread applications in mobile satellite communication and global positioning systems [14–26]. This work utilizes readily available paper as a substrate for a 3D-printed helical antenna, enabling cost-effective and accessible hands-on learning experiences for students in antenna design and fabrication [33].

The advent of artificial intelligence (AI) presents a transformative potential across various domains, including enhanced perception, communication, and medical diagnostics. Within the 9.4–10.8 GHz frequency band, also known as the X-band, AI technologies demonstrate significant promise in achieving these advancements [27, 28]. The X-band boasts unique characteristics that make it a perfect match for AI applications. Its exceptional bandwidth provides the information superhighway that AI algorithms crave, enabling the transmission of massive data streams at lightning speed. This bandwidth proves particularly crucial for applications that deal with complex data, such as medical imaging and remote sensing [29].

Furthermore, X-band signals travel long distances, making them ideal for satellite communication and radar systems. Here, AI steps in to revolutionize these domains. For instance, AI can analyse radar signals with unmatched precision, enabling the detection and classification of objects with pinpoint accuracy. This translates to superior target identification in various applications, from air traffic control to weather monitoring [30]. The integration of AI and X-band technology extends to the medical field as well. By analysing medical images acquired using X-band frequencies, AI algorithms can assist healthcare professionals in early disease detection and diagnosis. This can lead to improved patient outcomes and potentially save lives [31]. The impact of AI on X-band applications transcends various sectors. In remote sensing, AI algorithms can analyse X-band radar data to classify land cover, monitor environmental changes, and even aid in disaster response efforts [28, 29]. In essence, the X-band frequency band stands as a powerful platform poised to be supercharged by the transformative potential of AI. This synergy promises to usher in a new era of innovation across numerous disciplines, shaping a smarter and more sustainable future [28, 30, 32].

This paper presents a novel AI-enhanced, paper-based strip-helical antenna operating at the 9.4–10.8 GHz (X-band) frequency range. The antenna is fabricated by printing a conductive strip on a paper substrate and rolling it into a helical configuration, achieving circular polarization without complex matching networks. A significant gain enhancement, from 11.5 dBi to 15 dBi, is demonstrated through the application of a Grey Wolf Optimization (GWO) algorithm. This unique combination of a low-cost, eco-friendly paper substrate, AI-driven gain enhancement, and a simplified design offers a promising solution for diverse applications, including satellite communication, 5G, and select medical imaging modalities such as Magnetic Resonance Imaging (MRI), where the low-profile and potentially biocompatible nature of the paper substrate could be advantageous.

2. DESIGN OF HELICAL ANTENNA AND SPECIFICATIONS

Figure 1 depicts the geometrical configuration of the proposed strip helical antenna. This design involves a cylindrical helix constructed by patterning a metallic strip onto a paper substrate. The substrate, exhibiting a consistent strip width (w), is subsequently rolled into a hollow cylindrical form, resulting in a helical structure characterized by specific parameters: diameter (D), inter-turn spacing (S), turn length (L), and the number of turns (N). To facilitate axial-mode operation, a square ground plane (substrate B) is integrated beneath the helical structure. Table 1 provides a concise summary of the critical geometrical parameters of the helical antenna.

TABLE 1. Parameters of the proposed antenna.

Parameters	Width	Diameter	Spacing (center-to-center)
Short form	***W***	***D***	***S***
Parameters	Number of turns	Length of one turn	**-**
Short form	***N***	***L***	**-**

Empirical expressions for determining helical antenna parameters

$$D_o = \frac{15NSC^2}{\lambda_o^3}(dimensionless) \quad (1)$$

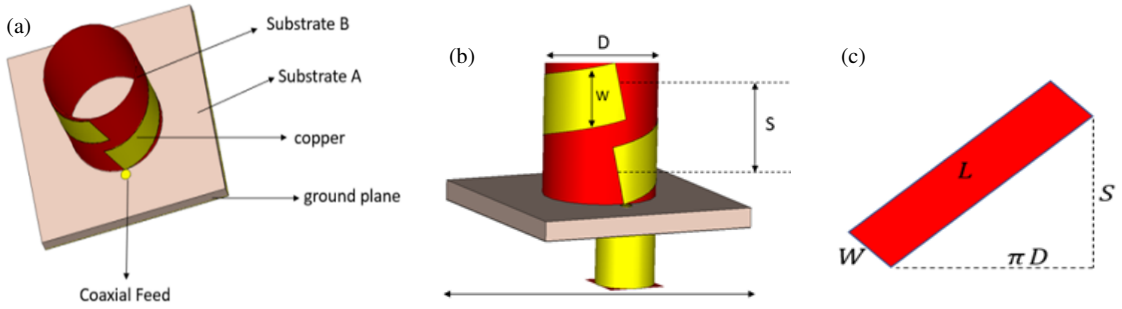

FIGURE 1. The proposed antenna design from various perspectives: (a) a three-dimensional view, (b) a side view, and (c) an unrolled view of a single helical turn.

In this context, D_0 represents the directivity, N the number of turns, S the spacing between turns, C the helix circumference, and λ the wavelength.

$$HPBW = \frac{52}{C}\sqrt{\frac{\lambda^2}{NS}}\,(degrees) \tag{2}$$

$$FNBW = \frac{115}{C}\sqrt{\frac{\lambda^a}{NS}}(degrees) \tag{3}$$

$$A_{eff} = \frac{C\lambda^2}{4\pi} meters^2 \tag{4}$$

$$Impedance\ at\ terminal = \frac{140C}{\lambda}\Omega \tag{5}$$

$$AR = \frac{2N+1}{2N} \tag{6}$$

In this context, *HPBW, FNBW, A_{eff}*, and *AR* are abbreviations for half-power beamwidth, first nulls beamwidth, effective aperture, and axial ratio, respectively. The ratio in question represents the quotient of the wave velocity along the helix to its velocity in free space:

$$p = \frac{\frac{L_o}{\lambda_o}}{\frac{s}{\lambda_o}+1} \tag{7}$$

The preceding analysis is relevant for standard end-fire radiation. In the case of Hansen-Woodyard end-fire radiation, the applicable equation is as follows:

$$p = \frac{\frac{L_o}{\lambda_o}}{\frac{s}{\lambda_o}+\left(\frac{2N+1}{2N}\right)} \tag{8}$$

According to [9] and [10], axial mode operation in helical antennas is achieved when the circumference (C) lies between $^3/_4\lambda$ and $^4/_3\lambda$.

Figure 2 illustrates the proposed helical antenna design, optimized for operation within the 9.4–10.8 GHz frequency band. This antenna incorporates 10 helical turns, carefully arranged to enhance radiation performance. Key dimensions include a wavelength (λ) of 30 mm, representing the distance travelled by a single cycle of the electromagnetic wave at the operating frequency, an overall length of 31.0 mm, a height of 70 mm, a turn spacing of 7 mm, and a helix diameter of 9.55 mm. These dimensions significantly influence the antenna's radiation pattern and overall performance characteristics.

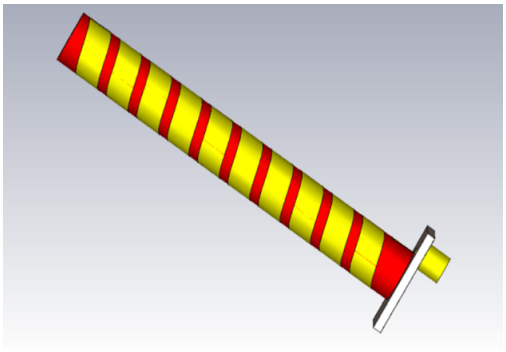

FIGURE 2. The proposed helical antenna design.

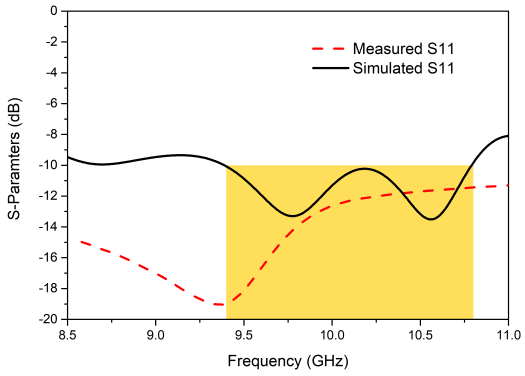

FIGURE 3. Simulated and measured S_{11} of the proposed Helical antenna design.

Table 2 summarizes the design parameters for a helical antenna operating within the 9.4–10.8 GHz frequency band. The selection of Teflon as the dielectric material and the incorporation of a square-shaped ground plane are design choices intended to optimize the antenna's performance characteristics, such as gain, bandwidth, and radiation efficiency.

TABLE 2. Design specification of the proposed helical antenna.

Parameter	Dielectric constant (ε_r)	Substrate thickness (h)	Pitch angle ($\propto$)	**Parameter**	The total length of the helical antenna (L)	Height of helical antenna (H)	Ground Plane (0.75λ)
Value	2.31	0.1 mm	13°	**Value**	310 mm	70 mm	22.5 mm
Parameter	Wavelength (λ)	Circumference (C)	Number of turns (N)	**Parameter**	Spacing between turns (S)	Cylindrical diameter (d)	Length of 1 turn strip (Lo)
Value	30 mm	30 mm	10	**Value**	7 mm	9.55 mm	31.0 mm

3. RESULTS AND DISCUSSION

Figure 3 illustrates the simulated and measured S_{11} parameters of the proposed helical antenna, designed to operate within the 9.4–10.8 GHz frequency band. The antenna exhibits a broad impedance bandwidth, extending from 9.4 GHz to 10.8 GHz, with a return loss (S_{11}) consistently below -10 dB across this range. A peak return loss of -13.6 dB is observed at 10.6 GHz, signifying effective impedance matching. This minimizes signal reflections, thereby maximizing power transfer and optimizing radiation efficiency. The measured S_{11}, also depicted in Figure 3, covers the target frequency band, although minor deviations from the simulated results are evident. These discrepancies can be attributed to variations introduced during the fabrication process, such as fabrication tolerances and inconsistencies in substrate permittivity, or potential mismatches encountered during the measurement procedure, including cable connections and calibration errors.

Axial ratio is a critical performance metric for circularly polarized antennas, with values significantly below -3 dB indicating high circular polarization purity. This study presents the design simulation and measurement of a helical antenna utilizing a paper substrate, intended for operation within the 9.4–10.8 GHz frequency band. Figure 4 depicts the simulated and measured axial ratio of the proposed antenna. The results indicate high circular polarization purity across a considerable portion of the operating band, with axial ratios maintained below -3 dB within the frequency band 9.4–10.8 GHz.

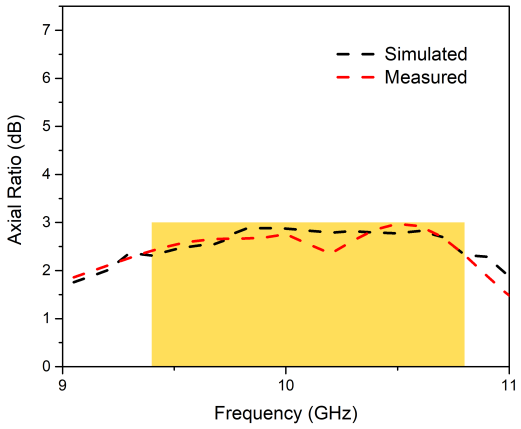

FIGURE 4. Axial ratio of the proposed 3D printed helical antenna.

The 5G helical antenna, fabricated using paper, demonstrated excellent impedance matching across the 9.4–10.8 GHz operating band. Measured voltage standing wave ratio (VSWR) values remained consistently low, averaging approximately 1.5, indicating efficient power transfer and minimal signal losses. Figure 5 graphically illustrates this, showing VSWR values consistently below 2 within the operating band. This wideband impedance matching is crucial for robust and efficient antenna performance, as it minimizes signal reflections and maximizes the amount of power radiated. Lower VSWR values generally correspond to improved antenna performance by minimizing reflected power and maximizing radiated power.

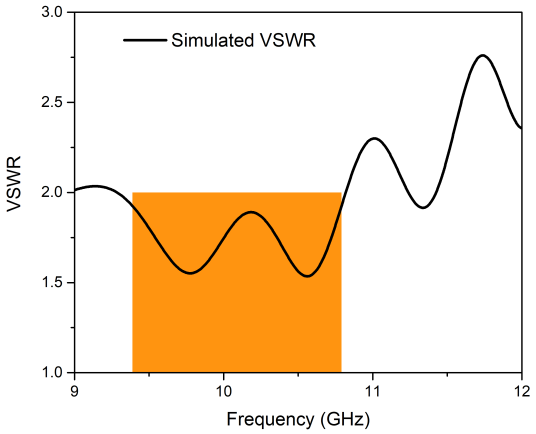

FIGURE 5. VSWR of the proposed 3D-printed helical antenna.

Figure 6 illustrates the simulated circular polarization (CP) gain of this antenna. A peak CP gain is observed at 9.8 GHz, indicative of efficient radiation and a well-focused radiation pattern at this frequency. A slight decrease in gain is observed beyond 10.3 GHz, potentially attributable to minor variations in radiation efficiency or a slight broadening of the radiation beamwidth [24]. The achieved CP gains, reaching 11.7 dBi at 9.7 GHz and 9.8 GHz, demonstrate the antenna's capability to effectively direct and concentrate radiated energy, crucial for maximizing signal strength in wireless communication systems. The compact size and simple design of the antenna offer advantages in terms of ease of fabrication, integration, and potential cost-effectiveness, making it a promising candidate for various applications in wireless communication and other fields.

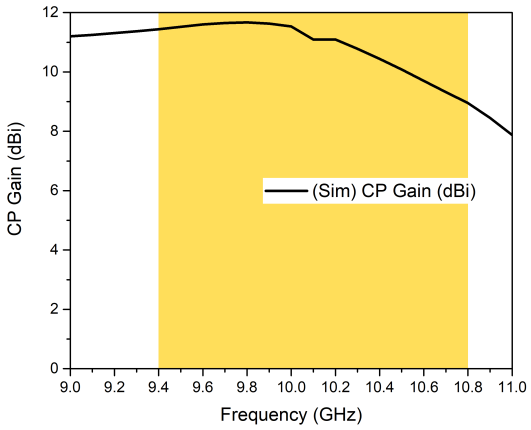

FIGURE 6. Simulated CP gain and directivity of the proposed 3D printed helical antenna.

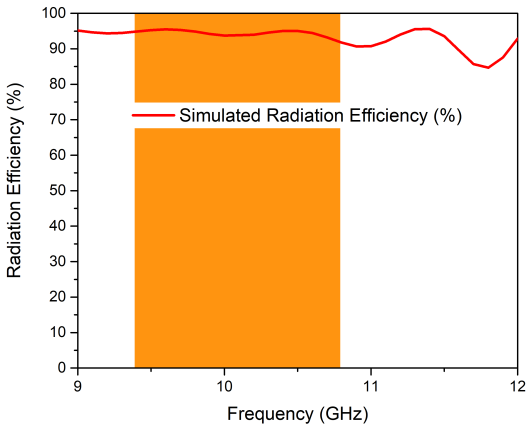

FIGURE 7. Simulated radiation efficiency of the proposed 3D printed helical antenna.

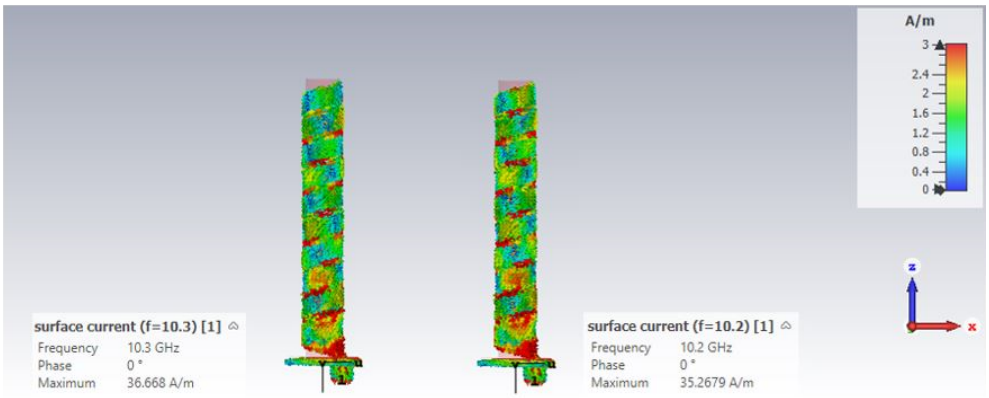

FIGURE 8. Surface current distribution of the proposed 3D-printed Helical antenna.

Figure 7 illustrates the simulated radiation efficiency of the proposed 3D-printed helical antenna. The results consistently demonstrate high radiation efficiency across the operating frequency band of 9.4 GHz to 10.8 GHz, ranging from 95% to 92%. This exceptional efficiency, particularly the peak value of 95%, is highly commendable for a 3D-printed helical antenna design. High radiation efficiency signifies that a significant portion of the input power is effectively converted into radiated electromagnetic waves, with minimal losses due to ohmic losses within the antenna structure or dielectric losses within the substrate material. This minimizes wasted energy and maximizes the power effectively transmitted into the surrounding environment. Such high efficiency is highly desirable for practical applications, including 5G wireless communication and satellite systems, as it directly translates to improved communication performance, enabling longer transmission distances, higher data rates, and enhanced signal quality [26].

Figure 8 illustrates the simulated surface current distribution on the helical antenna operating within the 9.4–10.8 GHz frequency band. The analysis reveals a peak surface current density of 35.2679 A/m at 10.2 GHz and 36.668 A/m at 10.3 GHz. A uniform current distribution is crucial for achieving efficient radiation and minimizing losses in any antenna. In the context of a helical antenna, a well-distributed current along the helix is essential for optimizing circular polarization, impedance matching, and overall radiation performance [36]. While the peak current density provides initial insights, a comprehensive analysis of the surface current distribution pattern is necessary to assess its suitability for 3D printing.

3D printing technologies often have limitations in terms of feature resolution, layer thickness, and material properties. These limitations can influence the accuracy of the fabricated structure and, consequently, the antenna's performance. By carefully analysing the surface current distribution and considering the limitations of the 3D printing process, necessary design adjustments can be made to mitigate potential issues and ensure optimal performance of the 3D-printed antenna.

Figure 9 depicts the 3D-printed helical antenna under test within a meticulously controlled anechoic chamber environment. To comprehensively characterize the antenna's radiation performance, a series of measurements were conducted. This experimental investigation aimed to meticulously quantify key radiation pattern characteristics, including beamwidth, side lobe levels, and polarization purity.

A meticulously calibrated measurement setup, comprising an anechoic chamber with specialized measurement equipment such as a vector network analyser and a turntable, was employed to ensure the acquisition of highly accurate and reliable measurement data. The anechoic chamber environment effectively minimizes the influence of external electromagnetic in-

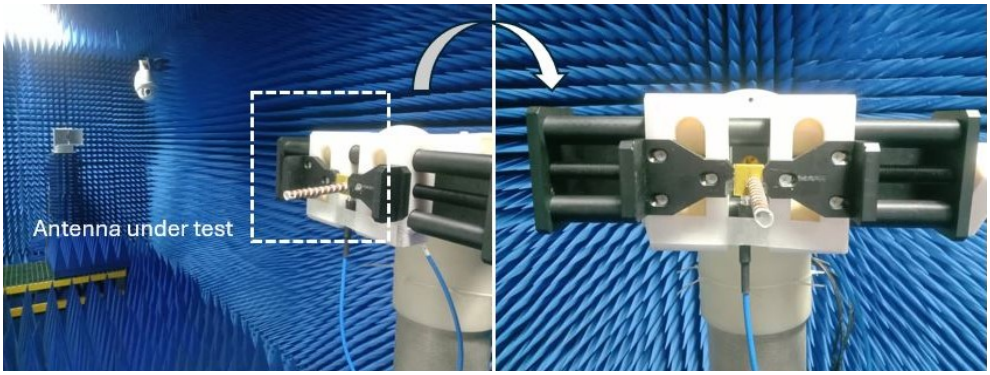

FIGURE 9. The proposed 3D printed helical antenna under test.

terference, while the specialized measurement equipment provides precise control over measurement parameters and facilitates the acquisition of high-fidelity data. This rigorous measurement methodology is essential for obtaining accurate and meaningful experimental results that can be used to validate the simulated performance of the 3D-printed helical antenna and assess its suitability for practical applications.

Experimental measurements revealed a peak CP gain of 11.6 dBi at 9.7 GHz, which, while being slightly lower than the simulated peak gain of 11.7 dBi at 9.7 GHz, demonstrates the antenna's capability to achieve significant gain in practical implementation as shown in Figure 10.

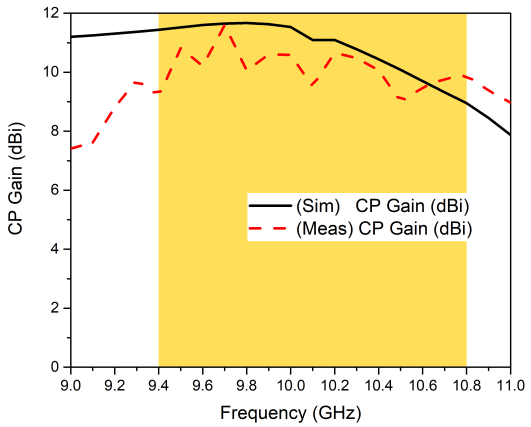

FIGURE 10. Simulated and measured CP gains of the proposed helical antenna.

The measured CP gain values provide insights into the antenna's radiation characteristics, suggesting a directional radiation pattern with potential for optimized performance in specific orientations. This directional characteristic has significant implications for the antenna's intended applications, as it can be strategically positioned to maximize signal strength and coverage in desired directions. To further enhance the antenna's performance beyond the measured results, this research leverages the power of Artificial Intelligence (AI) by employing the (GWO) algorithm. The details of the GWO algorithm implementation and the optimization results are presented in the AI section of this paper. The GWO algorithm is utilized to efficiently search the design space and identify optimal values for key parameters, such as the number of turns, helix pitch, and helix diameter, with the objective of achieving a target gain of 15 dBi at 10 GHz. This AI-driven optimization approach demonstrates the potential for significant performance improvements in helical antenna design.

Table 3 presents a comparison of the measured, simulated, and AI-optimized maximum gain values for the proposed helical antenna. This table provides valuable insights into the antenna's performance and the effectiveness of the AI-driven optimization process.

TABLE 3. The maximum gain results of the proposed antenna.

Parameter	Simulated	Measured	AI
Gain (dBi)	11.7	11.6	15

To validate the helical antenna's performance, its radiation patterns were measured. Figure 11 presents the normalized simulated and measured radiation patterns in circular polarization (RHCP and LHCP) at 9.8 GHz and 10.0 GHz. The measured patterns exhibit some asymmetry, particularly at 10.0 GHz in both RHCP and LHCP. The observed asymmetry is likely due to fabrication tolerances, variations in substrate material properties, imperfections in the feed structure, or the measurement environment. Discrepancies between simulated and measured patterns can also be attributed to measurement uncertainties and mismatches between simulated and actual antenna structures. Despite these discrepancies and the pattern asymmetry, the measured results demonstrate promising characteristics, including a wide bandwidth of 1.4 GHz. Future work will focus on minimizing the asymmetry through design modifications, including adjusting the feed point location, optimizing element spacing, incorporating a ground plane, investigating different substrate materials, and refining the mesh density in the simulation model. Despite the minor deviations and asymmetry, the measured results demonstrate the feasibility and potential of the proposed helical antenna for applications including satellite communication, 5G, and MRI. Future work will address the remaining challenges, including the pattern asymmetry, to further enhance performance and suitability for these applications [25, 37].

Table 4 presents a comparative analysis of existing helical antenna designs, encompassing a wide range of parame-

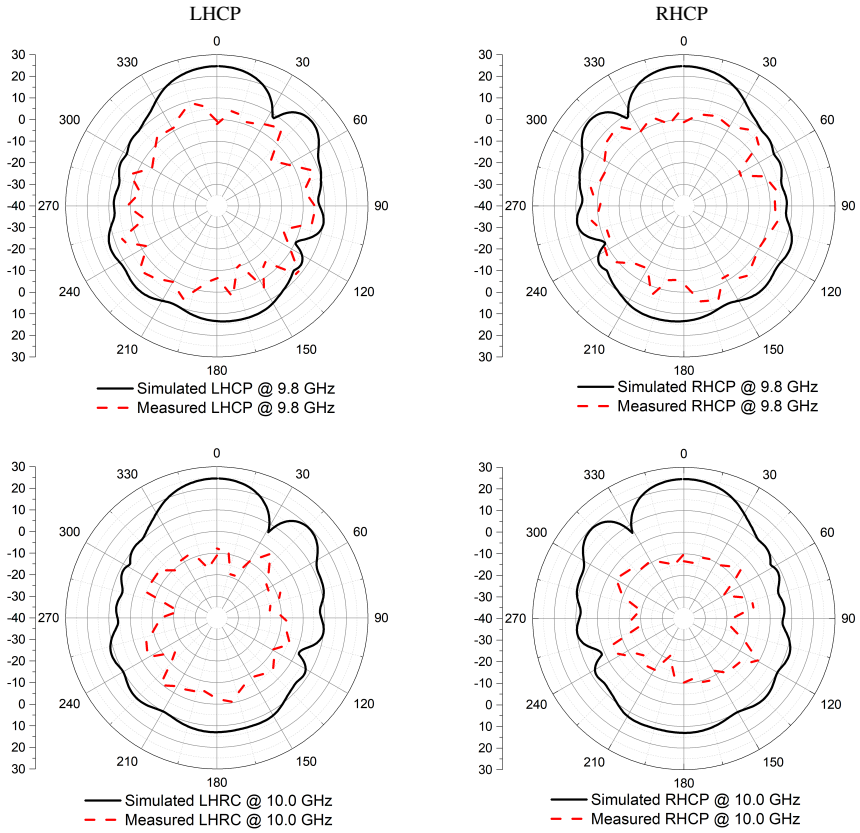

FIGURE 11. Simulated and measured polar radiation patterns at 9.8 GHz, and 10.0 GHz.

ters such as dimensions, feeding methods, and materials (copper, Paper). The operating frequencies of these antennas span across various bands, including X-band, satellite, Wi-Fi, and 5G. Researchers have extensively investigated key design factors, such as helix length, number of turns, and impedance matching techniques, to optimize antenna performance.

The proposed 3D-printed helical antenna, designed for operation within the 9.4 GHz to 10.8 GHz frequency band, demonstrates superior performance compared to several existing designs. Notably, it achieves a gain of 11.6 dBi at 9.8 GHz, exceeding the gain of 11.5 dBi reported at 7.5–10.5 GHz in [15] and some references [11, 14, 15, 17, 18, 20, 21], and [22]. The proposed antenna's key strengths include its compact size, simplicity of design, high gain, and high efficiency which is 95%.

Compared to the designs referenced in Table 4, the proposed antenna offers significant advantages. It exhibits superior gain performance and a more compact form factor than references [11, 17–19, 21, 22]. Furthermore, the proposed antenna demonstrates broader bandwidth capabilities, encompassing multiple bands including Wi-Fi, 5G, V2V, wideband, and satellite systems, surpassing the limited frequency coverage of references [11, 16, 18], and [21] in Table 4.

4. AI APPROACH FOR GAIN ENHANCEMENT FOR HELICAL ANTENNA

This paper investigates the application of the GWO, an AI-inspired algorithm, to enhance the gain of a helical antenna [35]. The GWO algorithm, inspired by the social hierarchy and hunting behavior of grey wolves, is employed to efficiently search the design space and identify optimal parameters for maximizing antenna peak CP gain. A simplified gain estimation model is used in conjunction with the GWO algorithm to determine the optimal values for key design parameters, namely the number of turns, helix pitch, and helix diameter. The optimization process aims to achieve a target gain of 15 dB at 10 GHz.

The methodology of the proposed algorithm where a simplified gain estimation model, as shown in Equation (1), is used to predict the antenna CP gain is based on the design parameters:

```
estimated_gain_db = 11 + 0.1 * N - 0.05 * P + 0.02 * D
```

where:

- N is the number of turns
- P is the helix pitch
- D is the helix diameter

This model provides a preliminary estimate of the antenna's performance and serves as a fitness function for the GWO algorithm. The GWO algorithm simulates the social hierarchy and hunting behaviour of grey wolves. A population of "wolves" is initialized within the defined search space. The algorithm then iteratively updates the position of each wolf based on the positions of the alpha, beta, and delta wolves (representing the leaders of the pack), as shown in Figure 12. This process guides the search towards optimal solutions within the design space.

TABLE 4. Previous work.

Ref.*	No. of turn/s*	BW* (GHz)	Peak CP* gain (dBi)	Rad. Eff* (%)	Size (mm)^2	Prototype	Application
14	1.5	8–12	8.17	-	$30 \times 30 \times 11.76$	Yes	X-band
11	4	1.56–2.93	11.3	-	$150 \times 150 \times 155$	Yes	L-Band, S-Band
15	8	7.5–10.5	11.5	-	$44 \times 72 \times 3.175$	Yes	X-band
16	10	9.5–10.5	11.6	-	$22.5 \times 22.5 \times 70$	Yes	X-band
17	10	4–6.7, 6.8–7.1	8.97	92	$38.80 \times 38.80 \times 120$	Yes	5G, sub-6 GHz band, C-band
18	1	5.75–5.85	6.96	73.2	$32 \times 32 \times 12$	Yes	aperture efficiency
19	10	4–6.51, 6.8–7.1	12.6	-	$38.80 \times 38.80 \times 120$	No	5G
20	2	5.05–7.05	5.7	95	$32 \times 32 \times 26.6$	Yes	Satellite, Wi-Fi
21	4	0.352–0.378	8	-	185×141	Yes	CubeSat-Satellite
22	10	4–8	11.53	99	129.31×64	No	5G
Proposed	**10**	**9.4–10.8**	**11.7**	**95**	**$70 \times 22.5 \times 22.5$**	**Yes**	**X-Band**
***Ref. = References, No*. of turn/s = Number of Turn/s, BW* = Bandwidth, CP* = Circular Polarization and Rad. Eff* (%) = Radiation Efficiency (%).**							

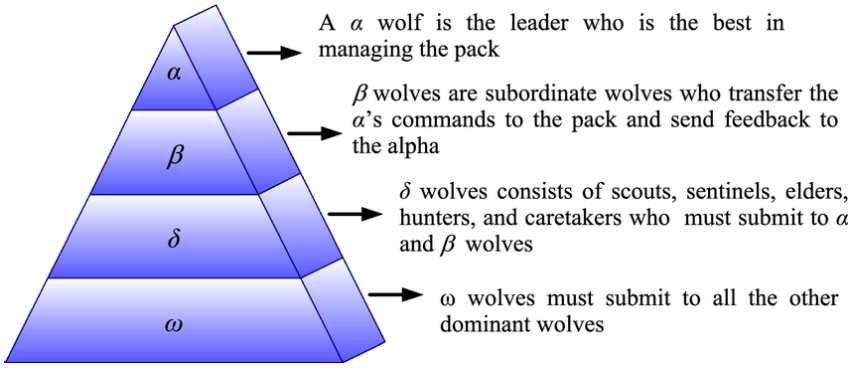

FIGURE 12. Hierarchy of grey wolf (dominance decreases from top down) [34].

The GWO algorithm was implemented in Python. The core components of the optimization process, including the

`calculate_gain`

function and the

`grey_wolf_optimizer`

The functions were implemented as described in the code snippet below:

```
# (Include a concise code snippet here, focusing on key aspects of the GWO algorit
#  - Initialization of wolves
#  - Updating wolf positions based on alpha, beta, and delta
#  - Fitness evaluation
#  - Boundary checks)
```

As the results of the proposed AI algorithm, the GWO algorithm provided results showcase the outcome of an antenna design optimization process. The best design parameters represent the optimal dimensions or other critical variables of the antenna structure, identified by the algorithm to achieve the most favourable performance. The specific interpretation of these values depends on the antenna type and the design variables used.

The optimization process resulted in the following optimal design parameters showing the best design parameters:

- Number of Turns (N): 11.94052785
- Helix Pitch (P): 8.10017905
- Helix Diameter (D): 11.21441828

The best fitness value of -30479.06 indicates that the estimated gain of the antenna with these parameters is close to the target gain of 15 dB. In this context, lower values (more negative) generally signify better performance.

As shown in Table 5, the antenna exhibits a peak gain of 15 dB at 10 GHz within the X-band (8–12 GHz). While demonstrating relatively consistent gain across the majority of the band, a notable dip is observed in the gain performance around

TABLE 5. Gain of the proposed helical antenna using AI (WGO).

Frequency (GHz)	8	8.33	8.67	9	9.33	9.67	10	10.33	10.67	11
Gain value (dBi)	12.48	12.48	12.48	11.98	11.98	11.98	15.00	11.78	11.78	11.78

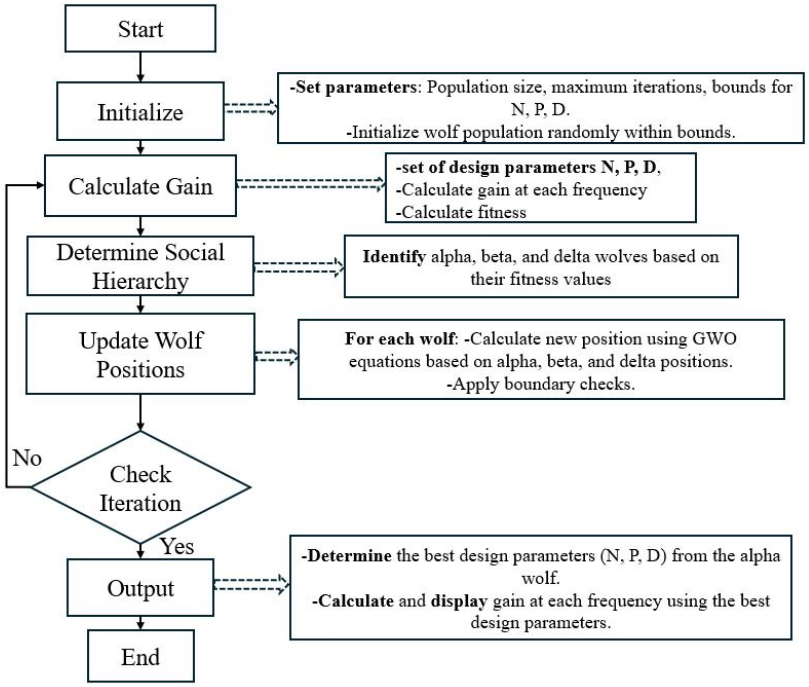

FIGURE 13. The process of optimizing the helical antenna using the Optimization of (GWO) algorithm.

9 GHz. This analysis suggests that the optimization process has yielded a promising antenna design with commendable overall performance within the X-band. However, the observed gain dip at 9 GHz necessitates further investigation and potential refinement of the design to ensure consistent and optimal performance across the entire operating frequency range [38].

Figure 13 shows the process of optimizing the proposed helical antenna using the Optimization of (G.W.O) algorithm. This flowchart provides a visual representation of the optimization process, highlighting the key steps and the role of the GWO algorithm in finding the optimal design parameters for the helical antenna.

Calculate the positions of each wolf in the population based on the positions of the alpha, beta, and delta wolves using the GWO equations:

$$X1 = \alpha\_pos - A1 * |C1 * \alpha\_pos - X| \quad (9)$$

$$X2 = \beta\_pos - A2 * |C2 * \beta\_pos - X| \quad (10)$$

$$X3 = \delta\_pos - A3 * |C3 * \delta\_pos - X| \quad (11)$$

$$X\_new = (X1 + X2 + X3)/3 \quad (12)$$

where:

X: Current position of the wolf

α_pos, β_pos, δ_pos: Positions of alpha, beta, and delta wolves

$A1$, $A2$, $A3$, $C1$, $C2$, $C3$: Coefficients determined by random numbers and the current iteration.

These equations guide the wolves in the population to move towards promising regions of the search space, influenced by the positions of the best solutions (alpha, beta, delta) found so far [39, 40]. The coefficients A and C introduce randomness and dynamically adjust the influence of the leaders throughout the optimization process.

This study demonstrates the successful application of the GWO algorithm for enhancing the gain of a helical antenna. The GWO algorithm effectively explored the design space and identified a set of optimal design parameters that aim to achieve the desired peak gain at a specific frequency. This research provides a foundation for further exploration and optimization of helical antenna designs using advanced optimization techniques AI.

5. CONCLUSION

In conclusion, this research successfully demonstrated the feasibility of a 3D-printed helical antenna for industrial applications operating within the 9.4–10.8 GHz frequency band. Experimental measurements revealed a peak CP gain of 11.6 dBi at 9.8 GHz, slightly below the simulated peak CP gain of 11.7 dBi at 9.8 GHz. To further enhance the antenna's performance, this research leveraged the power of Artificial Intelli-

gence (AI) by employing the Grey Wolf Optimization (GWO) algorithm. The GWO algorithm successfully optimized the antenna design, achieving a target gain of 15 dBi at 10 GHz, showcasing the significant potential of AI-driven optimization techniques for advancing the design of high-performance antennas for diverse industrial applications. Future research will explore design modifications to improve the radiation pattern symmetry, such as optimizing the feed structure and investigating alternative substrate materials. These efforts will further enhance the antenna's performance and broaden its potential applications.

ACKNOWLEDGEMENT

The study is funded by the Ministry of Higher Education (MOHE) of Malaysia through the Fundamental Research Grant Scheme (FRGS), No. FRGS/1/2023/TK07/UTEM/02/7. The author would also like to thank the Staff of UTeM for technical support.

REFERENCES

[1] Karami, F., P. Rezaei, A. Amn-E-Elahi, M. Sharifi, and J. S. Meiguni, "Efficient transition hybrid two-layer feed network: Polarization diversity in a satellite transceiver array antenna," *IEEE Antennas and Propagation Magazine*, Vol. 63, No. 1, 51–60, Oct. 2019.

[2] Taherkhani, M., J. Tayebpour, S. Radiom, and H. Aliakbarian, "Circularly polarised wideband quadrifilar helix antenna with ultra-wide beamwidth isoflux pattern for a S-band satellite ground station," *IET Microwaves, Antennas & Propagation*, Vol. 13, No. 10, 1699–1704, 2019.

[3] Shi, J., H. Liu, X. Wang, J. Zhang, F. Han, X. Tang, and J. Wang, "Miniaturized dual-resonant helix/spiral antenna system at MHz-band for FSK impulse radio intrabody communications," *IEEE Transactions on Antennas and Propagation*, Vol. 68, No. 9, 6566–6579, May 2020.

[4] Wang, S., L. Zhu, Y. Li, G. Zhang, J. Yang, J. Wang, and W. Wu, "Radar cross-section reduction of helical antenna by replacing metal with 3-D printed zirconia ceramic," *IEEE Antennas and Wireless Propagation Letters*, Vol. 19, No. 2, 350–354, Dec. 2019.

[5] Karami, F., P. Rezaei, A. Amn-E-Elahi, Z. Mousavirazi, T. A. Denidni, and A. A. Kishk, "A compact high-performance patch array with suppressed cross polarization using image feed configuration," *AEU — International Journal of Electronics and Communications*, Vol. 127, 153479, 2020.

[6] Hosseini, M., M. Hakkak, and P. Rezaei, "Design of a dual-band quadrifilar helix antenna," *IEEE Antennas and Wireless Propagation Letters*, Vol. 4, 39–42, Jun. 2005.

[7] Yang, Y.-H., J.-L. Guo, B.-H. Sun, and Y.-H. Huang, "Dual-band slot helix antenna for global positioning satellite applications," *IEEE Transactions on Antennas and Propagation*, Vol. 64, No. 12, 5146–5152, Dec. 2016.

[8] Yuan, J., K. Qiu, and Z. Chen, "A compact helix antenna with wide axial ratio bandwidth using a spiral microstrip coupling feedline for GNSS applications," *IEEE Antennas and Wireless Propagation Letters*, Vol. 20, No. 4, 433–437, Jan. 2021.

[9] Chen, Z. and Z. Shen, "Wideband flush-mounted surface wave antenna of very low profile," *IEEE Transactions on Antennas and Propagation*, Vol. 63, No. 6, 2430–2438, Mar. 2015.

[10] Zeain, M. Y., M. Abu, Z. Zakaria, A. J. A. Al-Gburi, R. Syahputri, A. Toding, and S. Sriyanto, "Design of a wideband strip helical antenna for 5G applications," *Bulletin of Electrical Engineering and Informatics*, Vol. 9, No. 5, 1958–1963, Aug. 2020.

[11] Siahcheshm, A., J. Nourinia, C. Ghobadi, and M. Shokri, "Circularly polarized printed helix antenna for L- and S-bands applications," *Radioengineering*, Vol. 29, No. 1, 67–73, Apr. 2020.

[12] Cheng, Z. W., J. Deng, M. Wang, J. R. Chen, S. Wang, S. Luan, X. Liu, F. Gao, H. F. Ma, and T. J. Cui, "A compact axial-mode helical antenna based on spoof surface plasmon polaritons," *IEEE Transactions on Antennas and Propagation*, Vol. 71, No. 7, 5582–5590, Apr. 2023.

[13] Kong, G., X. Li, Q. Wang, and J. Zhang, "A wideband reconfigurable dual-branch helical reflectarray antenna for high-power microwave applications," *IEEE Transactions on Antennas and Propagation*, Vol. 69, No. 2, 825–833, Aug. 2020.

[14] Zhao, L., C. Liu, C. Li, D. Song, Y. Wang, Y. Liang, H. Zhao, and C. Hu, "A novel helical antenna for high-power design in X-band," *AEU — International Journal of Electronics and Communications*, Vol. 168, 154725, 2023.

[15] Zainud-Deen, S. H., H. A. E.-A. Malhat, N. A. A. S. El-Shalaby, and S. M. Gaber, "Circular polarization bandwidth reconfigurable high gain planar plasma helical antenna," *IEEE Transactions on Plasma Science*, Vol. 47, No. 9, 4274–4280, Aug. 2019.

[16] Zeain, M. Y., M. Abu, Z. Zakaria, H. S. M. Sariera, and H. Lago, "Design of helical antenna for wideband frequency," *International Journal of Engineering Research and Technology*, Vol. 11, No. 4, 595–603, 2018.

[17] Zeain, M. Y., Z. Zakaria, M. Abu, A. J. A. Al-Gburi, H. Alsariera, A. Toding, S. Alani, M. A. Al-Tarifi, O. S. Al-Heety, H. Lago, and T. Saeidi, "Design of helical antenna for next generation wireless communication," *Przegląd Elektrotechniczny*, Vol. 11, 96–99, 2020.

[18] Ni, T., B. Wang, M. Wang, P. Wu, X. Wang, and Q. Liu, "A radial line array with cylindrical-hole probe-fed helical elements for enhancing aperture efficiency and power-handling capacity," *IEEE Antennas and Wireless Propagation Letters*, Vol. 23, No. 2, 718–722, Nov. 2023.

[19] Zeain, M. Y., M. Abu, Z. Zakaria, A. J. A. Al-Gburi, R. Syahputri, A. Toding, and S. Sriyanto, "Design of a wideband strip helical antenna for 5G applications," *Bulletin of Electrical Engineering and Informatics*, Vol. 9, No. 5, 1958–1963, Aug. 2020.

[20] Amn-E-Elahi, A., P. Rezaei, F. Karami, F. Hyjazie, and H. Boutayeb, "Analysis and design of a stacked PCBs-based quasi-helix antenna," *IEEE Transactions on Antennas and Propagation*, Vol. 70, No. 12, 12 253–12 257, Sep. 2022.

[21] Costantine, J., Y. Tawk, I. Maqueda, M. Sakovsky, G. Olson, S. Pellegrino, and C. G. Christodoulou, "UHF deployable helical antennas for CubeSats," *IEEE Transactions on Antennas and Propagation*, Vol. 64, No. 9, 3752–3759, Jun. 2016.

[22] Paul, P., A. K. Roy, N. Bhowmike, M. N. Islam, and X. Liu, "Design and simulation of a monofilar helical antenna for 5G and beyond applications," in *2024 IEEE International Symposium on Measurements & Networking (M&N)*, 1–6, Rome, Italy, 2024.

[23] Zeain, M. Y., M. Abu, and S. N. Zabri, "Investigation of printed helical antenna using varied materials for ultra-wide band frequency," *Journal of Telecommunication, Electronic and Computer Engineering (JTEC)*, Vol. 10, No. 2–7, 137–142, Jul. 2018.

[24] Zeain, M. Y., M. Abu, A. A. Althuwayb, H. Alsariera, A. J. A. Al-Gburi, A. A. Abdulbari, and Z. Zakaria, "A new technique of FSS-based novel chair-shaped compact MIMO antenna to enhance the gain for sub-6 GHz 5G applications," *IEEE Access*, Vol. 12, 49 489–49 507, 2024.

[25] Constantinides, A., C. Kousioumari, S. Najat, and H. Haralambous, "Low-profile circularly polarized HF helical phased array: Design, analysis, and experimental evaluation," *Applied Sciences*, Vol. 14, No. 12, 5075, Jun. 2024.

[26] Georgakopoulos, S. V., C. L. Zekios, A. Sattar-Kaddour, M. Hamza, A. Biswas, B. Clark, C. Ynchausti, L. L. Howell, S. P. Magleby, and R. J. Lang, "Origami antennas," *IEEE Open Journal of Antennas and Propagation*, Vol. 2, 1020–1043, 2021.

[27] Seidaliyeva, U., L. Ilipbayeva, K. Taissariyeva, N. Smailov, and E. T. Matson, "Advances and challenges in drone detection and classification techniques: A state-of-the-art review," *Sensors*, Vol. 24, No. 1, 125, 2024.

[28] Cayamcela, M. E. M. and W. Lim, "Artificial intelligence in 5G technology: A survey," in *2018 International Conference on Information and Communication Technology Convergence (ICTC)*, 860–865, Jeju, Korea (South), Oct. 2018.

[29] Congalton, R. G., "Remote sensing and image interpretation," *Photogrammetric Engineering & Remote Sensing*, Vol. 81, No. 8, 615–616, Aug. 2015.

[30] Goldstein, J. S., "Introduction to radar systems third edition [Book Review]," *IEEE Aerospace and Electronic Systems Magazine*, Vol. 16, No. 10, 19–19, Oct. 2001.

[31] Hamet, P. and J. Tremblay, "Artificial intelligence in medicine," *Metabolism*, Vol. 69, S36–S40, Apr. 2017.

[32] Nabwy, H. H., S. M. Ali, M. M. Khafagy, S. A. El-Tohamy, B. S. Mohamed, S. E. E. Mohamed, and A. M. Mohamed, "Optimized helical antenna for wireless application at 2.4 GHz using gray wolf optimizer," in *Proceedings of the 9th International Conference on Advanced Intelligent Systems and Informatics*, 432–443, 2023.

[33] Singh, A. K., S. K. Mahto, R. Sinha, M. Alibakhshikenari, A. J. A. Al-Gburi, A. Ahmad, L. Kouhalvandi, B. S. Virdee, and M. Dalarsson, "Low-loss paper-substrate triple-band-frequency reconfigurable microstrip antenna for sub-7 GHz applications," *Sensors*, Vol. 23, No. 21, 8996, Nov. 2023.

[34] Pham, A.-D., N.-T. Ngo, Q.-T. Nguyen, and N.-S. Truong, "Hybrid machine learning for predicting strength of sustainable concrete," *Soft Computing*, Vol. 24, No. 19, 14 965–14 980, Mar. 2020.

[35] Mirjalili, S., S. M. Mirjalili, and A. Lewis, "Grey wolf optimizer," *Advances in Engineering Software*, Vol. 69, 46–61, 2014.

[36] Alsariera, H., Z. Zakaria, and A. A. M. Isa, "A broadband P-shaped circularly polarized monopole antenna with a single parasitic strip," *IEEE Antennas and Wireless Propagation Letters*, Vol. 18, No. 10, 2194–2198, Oct. 2019.

[37] Zhang, Y., H. Wang, D. Liao, and W. Fu, "Phase-tuning metasurface for circularly polarized broadside radiation in broadband," *Scientific Reports*, Vol. 8, No. 1, 2970, Feb. 2018.

[38] Li, Y., X. Lin, and J. Liu, "An improved gray wolf optimization algorithm to solve engineering problems," *Sustainability*, Vol. 13, No. 6, 3208, 2021.

[39] Momanyi, E. and D. Segera, "A master-slave binary grey wolf optimizer for optimal feature selection in biomedical data classification," *Biomed Research International*, Vol. 2021, No. 1, 5556941, Oct. 2021.

[40] Rezaei, H., O. Bozorg-Haddad, and X. Chu, "Grey wolf optimization (GWO) algorithm," *Advanced Optimization by Nature-Inspired Algorithms*, 81–91, 2017.